Supporting Information

Single O atom doped Ag cluster cations for CO oxidation: A superatom $Ag_{15}O^+$ with endohedral O

Qiuying Du[1, §], Jin Hu[2, §], Xiaopeng Xing[2], Si Zhou[1*], Jijun Zhao[1*]*

[1]Key laboratory of Material Modification by Laser, Ion and Electron Beams (Dalian University of Technology), Ministry of Education, Dalian 116024, China

[2] School of Chemical Science and Engineering, Shanghai Key Lab of Chemical Assessment and Sustainability, Tongji University, 1239 Siping Road, Shanghai 200092, China

Details of computational methods:

The comprehensive genetic algorithm (CGA) operated on Gaussian16[1] package was used to unbiased global search the structures of Ag_nO^+ (n = 7−11, 15, 19, 22) clusters. The cam-B3LYP functional and LanL2DZ basis set were used for structure optimization during each step of CGA. At the beginning of CGA search, sixteen isomers were generated randomly as initial populations of Ag_nO^+ (n = 7−11, 15, 19, 22) clusters. Each child structure was produced by mating, mutation, or exchanges the atomic type of a pair of atoms operations with probability of 40, 20 and 40 percent, respectively. Three thousand iterations were lasted up to ensure getting the global minimum on the potential energy surface for each Ag_nO^+ cluster. More details of CGA can be found in a review article.[2] The low-energy isomers from CGA were re-optimized by using a higher-level cam-B3LYP/SDD method to distinct the final lowest-energy structure of clusters.

As for interactions between Ag_nO^+ (n = 7−10, 15) clusters with CO, we employed the aug-cc-pVDZ-pp basis set for Ag and the 6-311G(d) basis set for C and O respectively accompanied with cam-B3LYP functional considering the Grimme's semiempirical D3 dispersion correction. For both structure optimization and kinetic barrier calculations, the thermal effect (240K) was considered by including zero point energy and entropy correction to the total energy. Transition states and kinetic barriers for CO oxidation were obtained by Berny algorithm. The obtained reactants, intermediates, final product structures and transition states were confirmed by analyzing their vibrational modes, which have no and only one imaginary frequency, respectively. Charger distributions of structures were obtained by using natural population analysis (NPA). The feasibility of cam-B3LYP functional combined with LanL2DZ, SDD, and aug-cc-pVDZ-pp basis sets were supported by benchmark calculations for Ag_2 dimer in Table S1 of Supporting Information.

Using the initial structures from Gaussian16, total energies considered scalar-relativistic effect based on the zero order regular approximation (ZORA) were performed by using ADF 2018.104 package.[3-5] The cam-B3LYP functional accompanied with the all-electron Slater basis set of triple-zeta with polarization

function (TZP) was employed for calculating pristine Ag_nO^+ clusters. In addition, the Grimme's semiempirical D3 dispersion correction was considered for calculating the interaction between Ag_nO^+ clusters with CO. The interaction and chemical bonding nature between the O species and Ag_n^+ fragment of each Ag_nO^+ clusters, Ag_nO^+ cluster and CO molecule were described using the energy decomposition analysis and natural orbitals for chemical valence (EDA-NOCV) method.[6-8] From EDA, the total bonding energy can be divided into three parts:

$$\Delta E_{int} = \Delta E_{pauli} + \Delta E_{elstat} + \Delta E_{oi} \quad (s1)$$

ΔE_{pauli} is the repulsion energy caused by the Pauli exclusion principle between two fragments, ΔE_{elstst} and ΔE_{oi} are the attraction energies from electrostatic and orbital interactions between two fragments, respectively.

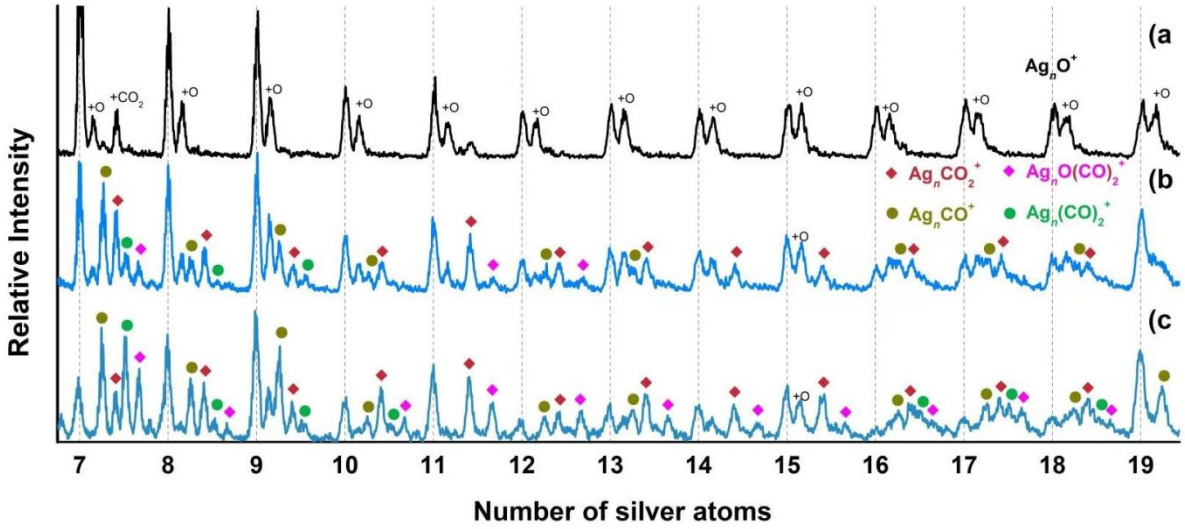

Figure S1. Mass spectra of Ag_nO^+ (n = 7−19) (a) and their reaction products after exposure to different quantity of CO gas with flow rates of (b) 0.025 sccm and (c) 0.05 sccm at 200 K.

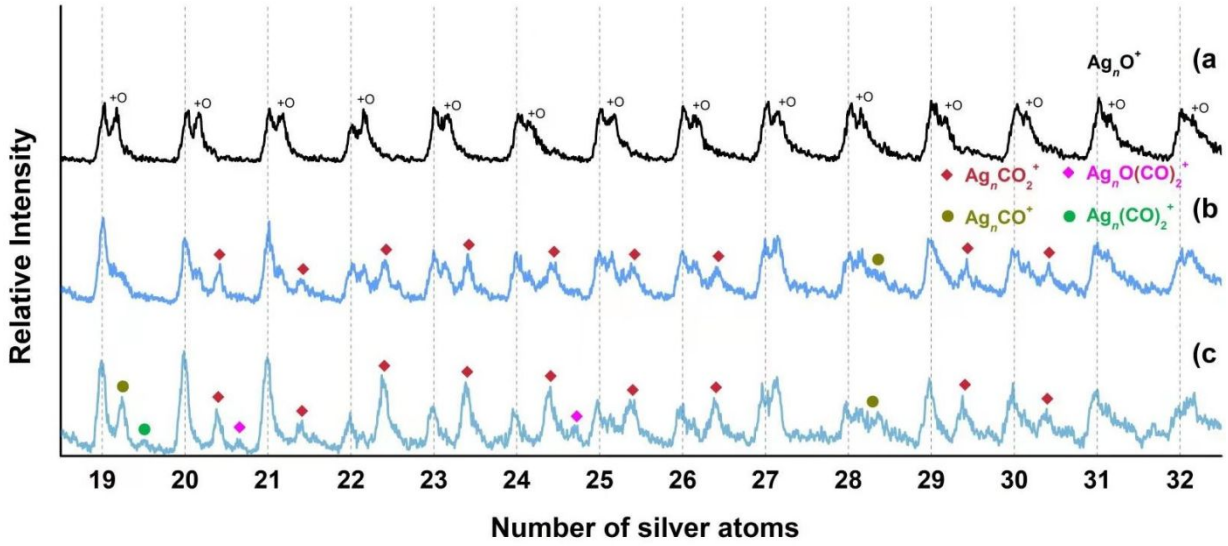

Figure S2. Mass spectra of Ag_nO^+ (n = 19−32) (a) and their reaction products after exposure to different quantity of CO gas with flow rates of (b) 0.025 sccm and (c) 0.050 sccm at 200 K.

Figure S1 and S2 show the reaction products of Ag_nO^+ (n = 7−19) and Ag_nO^+ (n = 19−32) at 200 K. In Figure S1, most Ag_n^+ and Ag_nO^+ combine one or two CO molecules, forming species with the formula of Ag_nCO^+, $Ag_n(CO)_2^+$, $Ag_nCO_2^+$ and $Ag_nO(CO)_2^+$. For the larger clusters shown in Figure S2, the CO adsorption species are not as abundant as those shown in Figure S1, and only a few clusters form products containing two CO molecules. It is also found that the intensities of products with multiple CO molecules and several ones with only on CO molecule increase with decreasing the temperature, and vice versa. In addition, the abundances of these products decrease with increasing cluster sizes on which the positive charge is more dispersed. The effects of temperature and the cluster size indicate that they are stabilized by electrostatic physisorption interactions rather than chemical bonding interactions.

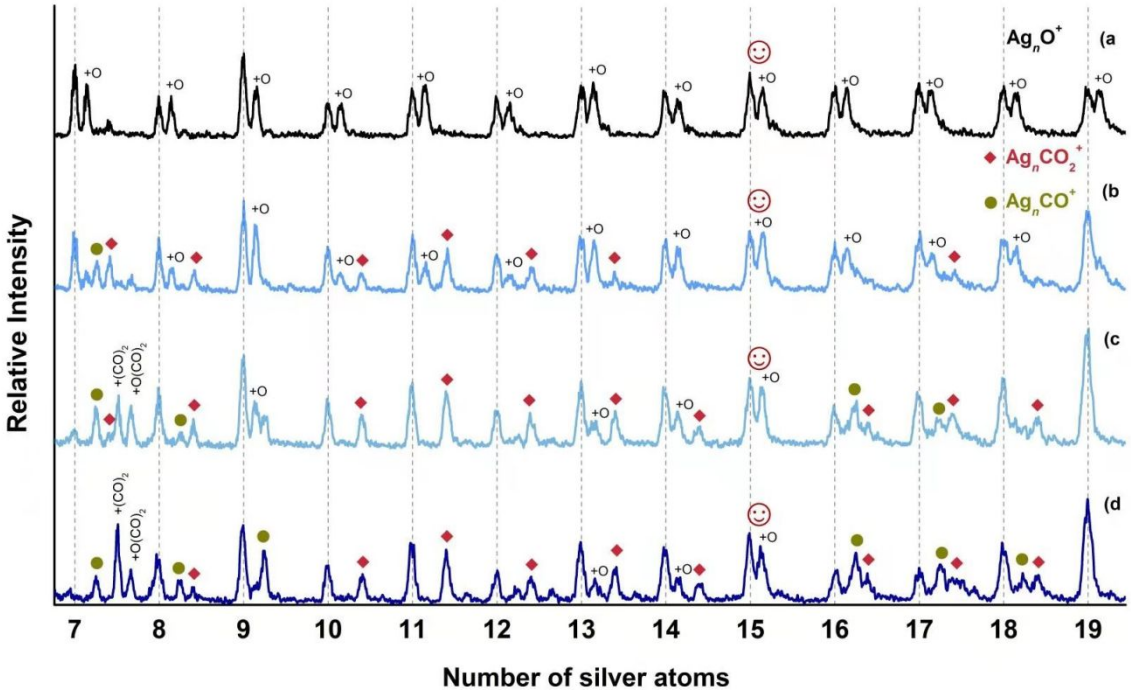

Figure S3. Mass spectra of Ag_nO^+ (n = 7−19) (a) and their reaction products after exposure to different quantity of CO gas with flow rates of (b) 0.025 sccm, (c) 0.100 sccm and (d) 0.200 sccm at 240 K. The smiling face marked the cluster that is inert toward CO.

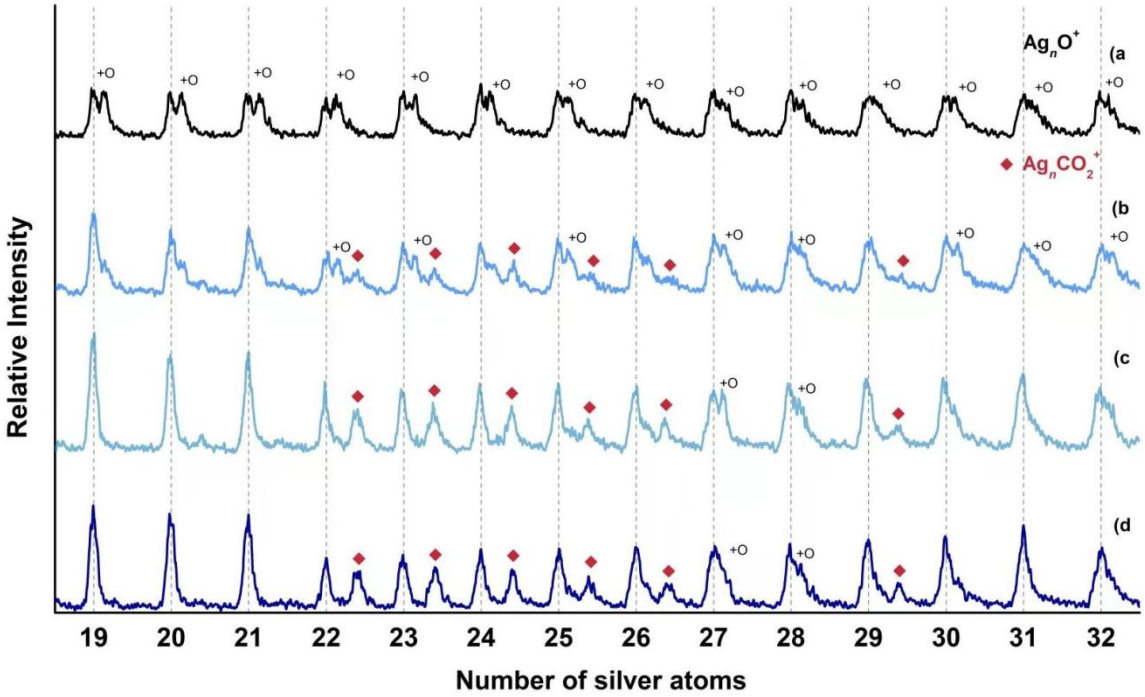

Figure S4. Mass spectra of Ag_nO^+ (n = 19−32) (a) and their reaction products after exposure to different quantity of CO gas with flow rates of (b) 0.025 sccm, (c) 0.100 sccm and (d) 0.200 sccm at 240 K.

Figure S3 and S4 showe the reaction products of Ag_nO^+ (n = 7−19) and Ag_nO^+ (n = 19−32) at 240 K. At this temperature, the CO adsorption processes due to weak physisorption interactions are largely suppressed. The products containing more than one CO molecules are only observed on the clusters Ag_7 and Ag_7O^+, on which the positive charge is more concentrated than those on the large sizes. The suppression of physisorption processes at 240 K made it easy to distinguish the products from chemical reactions between this unique Ag_nO^+ cluster series and single CO. The reaction characters of all Ag_nO^+ (n = 7−32) can be summarized as follows:

Mechanism (I) $Ag_nO^+ + CO = Ag_nCO_2^+$

n = 7, 8, 10, 11, 12, 13, 14, 17, 18, 22−26, and 29;

Mechanism (II) $Ag_nO^+ + CO = Ag_n^+ + CO_2$

n = 8, 9, 16, 17, 18, 19, 20, 21, 30, 31, and 32;

Relatively inert sizes n = 15, 27, and 28.

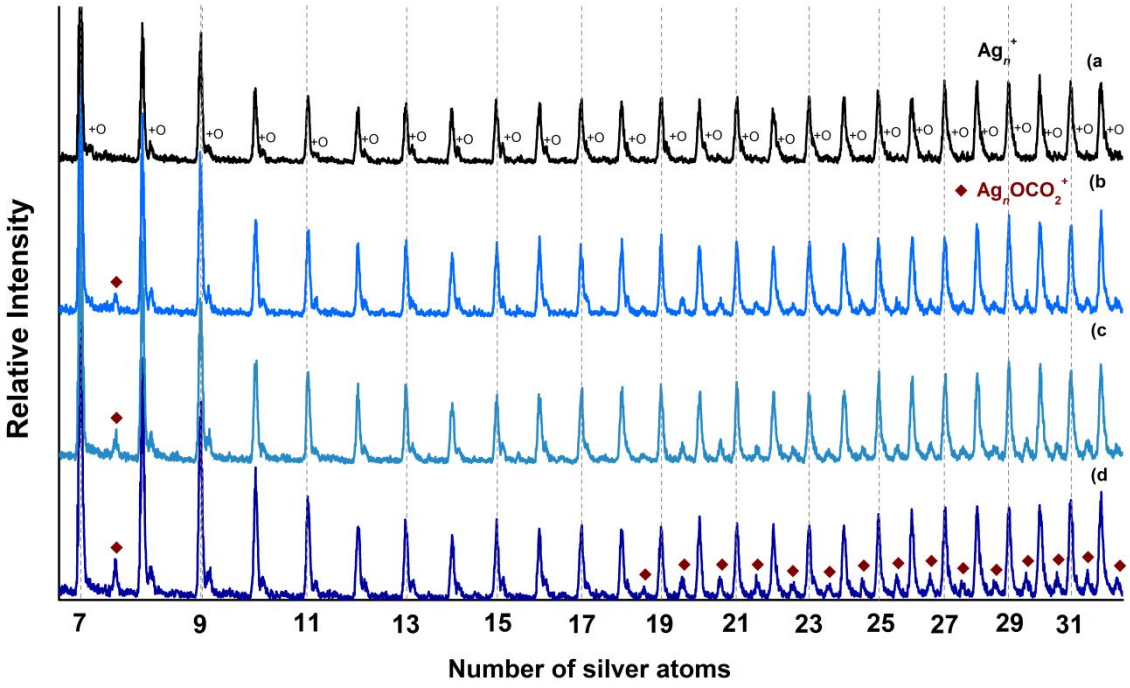

Figure S5. Mass spectra of Ag_n^+ (n = 7−32) (a) and the clusters after exposure to different quantity of CO_2 gas with flow rates of (b) 1.00 sccm, (c) 4.00 sccm and (d) 12.00 sccm at 225 K. No $Ag_nCO_2^+$ (n = 7−32) products were observed even though the CO_2 flow rates were much higher and the temperature was lower than the parameters used in Figure S4. This indicates there should be a barrier from free CO_2 molecules to the CO_2 units of all $Ag_nCO_2^+$ presented in Figure S4, i.e., their CO_2 units were chemically bonded. Weak Ag_nO^+ (n = 7−32) peaks appeared in (a) because of background oxygen not completely cleaned after the previous experiments, which formed the $Ag_nOCO_2^+$ series in (b)-(d) in reactions with CO_2.

Table S1. Error between calculated bond length (δ_R, in Å) and frequency (δ_ω, in cm^{-1}) with different functional basis set combinations and experimental values of Ag_2 dimer.[9-10]

	LanL2DZ		Lanl2TZ		SDD		cc-PVTZ-pp		def2-TZVPP		dhf-TZVP		aug-cc-pVDZ-pp		aug-cc-pVTZ-pp	
	δ_R	δ_ω	δ_R	δ_ω	δ_R	δ_ω	δ_R	δ_ω	δ_R	δ_ω	δ_R	δ_ω	δ_R	δ_ω	δ_R	δ_ω
B3LYP	0.08	-14.67	0.08	-15.77	0.06	-12.74	0.06	-12.77	0.06	-15.4	0.06	-14.44	0.06	-14.06	0.05	-12.43
cam-B3LYP	0.06	-2.31	0.05	-2.48	**0.04**	**0.34**	0.03	-2.42	0.04	-4.51	0.03	-3.18	**0.03**	**-3.15**	0.03	-1.95
B3PW91	0.06	-7.17	0.06	-8.76	0.04	-5.53	0.04	-7.56	0.04	-9.57	0.04	-8.17	0.04	-7.71	0.03	-6.65
PW91	0.05	-5.15	0.05	-6.54	0.04	-3.23	0.03	-5.57	0.03	-7.81	0.03	-6.33	0.03	-5.63	0.02	-4.35
O3LYP	0.11	-30.45	0.10	-30	0.08	-25.26	0.08	-24.2	0.08	-25.64	0.07	-24.02	0.07	-23.68	0.06	-22.43
X3LYP	0.08	-14.33	0.08	-15.36	0.06	-12.12	0.06	-12.58	0.06	-14.32	0.06	-13.47	0.06	-13.21	0.05	-11.97
HSE06	0.06	-7.45	0.06	-8.8	0.05	-5.42	0.04	-7.62	0.04	-9.18	0.04	-7.84	0.04	-7.48	0.03	-6.63
M06	0.06	-6.09	0.07	-11.93	0.06	-7.33	0.06	-2.35	0.06	-3.65	0.06	-3.06	0.06	-2.44	0.06	-2.35
M06-L	0.04	3.30	0.06	-7.81	0.04	-5.21	0.05	-12.3	0.05	-12.92	0.04	-11.88	0.04	-11.02	0.05	-12.3
M06-2X	0.15	-29.72	0.15	-29.46	0.15	-31.82	0.14	-38.95	0.14	-40.09	0.14	-39.55	0.14	-39.91	0.14	-38.95
PBE	0.06	-7.32	0.06	-8.62	0.04	-5.92	0.04	-7.51	0.04	-9.6	0.03	-8.07	0.03	-7.52	0.04	-7.51
PBE0	0.06	-8.66	0.06	-9.29	0.05	-6.09	0.04	-8.28	0.04	-9.92	0.04	-8.28	0.04	-8.23	0.04	-8.28
BP86	0.05	-3.14	0.05	-5.91	0.04	-2.87	0.03	-4.71	0.03	-7.31	0.03	-5.8	0.03	-5.07	0.03	-4.71
TPSSh	0.05	-2.53	0.05	-3.67	0.03	-0.38	0.03	-3.56	0.03	-5.51	0.02	-4.16	0.02	-3.55	0.03	-3.56

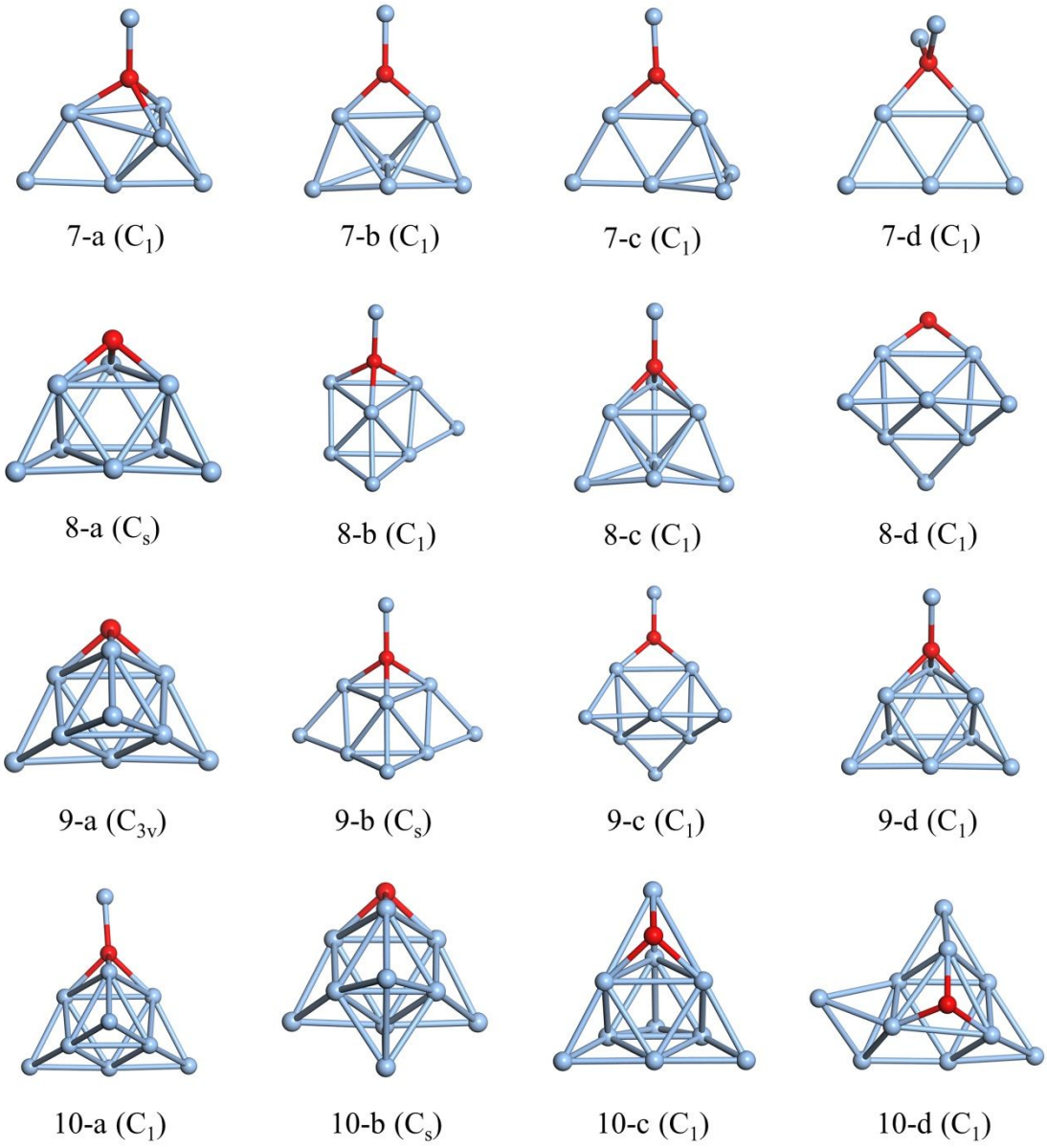

Figure S6. Low-energy structures of $Ag_{7-10}O^+$ clusters. For each size *n*, the isomers were marked as *n*-b, *n*-c, *n*-d relating to the energy difference with the lowest-energy one (marked as *n*-a). The cluster symmetries are given in brackets. The sliver and oxygen atoms are shown in blue and red, respectively.

Table S2. The geometric and electronic properties of $Ag_{7-10}O^+$ clusters from cam-B3LYP/SDD calculation considering zero point and thermal correction, including energy difference between isomers with G-S at each size *n* (ΔE_{GS}), binding energy per atom (E_b), HOMO-LUMO gap (E_{HL}), average bond length between Ag and O (R_{Ag-O}), average bond length between Ag and Ag (R_{Ag-Ag}), and minimum frequency (υ_{min}).

Cluster	ΔE_{GS} (eV)	E_b (eV)	E_{HL} (eV)	R_{Ag-O} (Å)	R_{Ag-Ag} (Å)	υ_{min} (cm^{-1})
7-a	**0.000**	**0.710**	**4.500**	**2.189**	**2.860**	**30.75**
7-b	0.116	0.696	4.590	2.076	2.842	20.36
7-c	0.144	0.692	4.436	2.070	2.805	17.56
7-d	0.275	0.676	3.405	2.159	3.103	11.12
8-a	**0.000**	**0.776**	**3.728**	**2.144**	**2.883**	**41.09**
8-b	0.039	0.771	3.374	2.169	2.853	19.71
8-c	0.109	0.764	3.265	2.178	2.874	26.14
8-d	0.143	0.760	4.844	2.155	2.823	21.23
9-a	**0.000**	**0.944**	**4.871**	**2.120**	**2.861**	**50.87**
9-b	0.183	0.925	4.408	2.162	2.836	16.85
9-c	0.296	0.914	4.844	2.070	2.814	12.75
9-d	0.393	0.904	3.674	2.186	2.863	29.50
10-a	**0.000**	**0.976**	**2.585**	**2.162**	**2.856**	**24.35**
10-b	0.153	0.962	3.265	2.148	2.879	22.32
10-c	0.248	0.954	3.510	2.126	2.901	-9.62
10-d	0.282	0.951	3.075	2.114	2.885	14.13

Table S3. Energy difference (in eV) between higher spin states relative to the lowest spin state (singlet state for odd *n* and doublet state of even *n*) of Ag_nO^+ clusters.

Cluster	triplet	quintuplet
Ag_7O^+	1.86	3.20
Ag_9O^+	1.51	3.06
	quartet	sextet
Ag_8O^+	1.51	3.79
$Ag_{10}O^+$	2.28	3.52

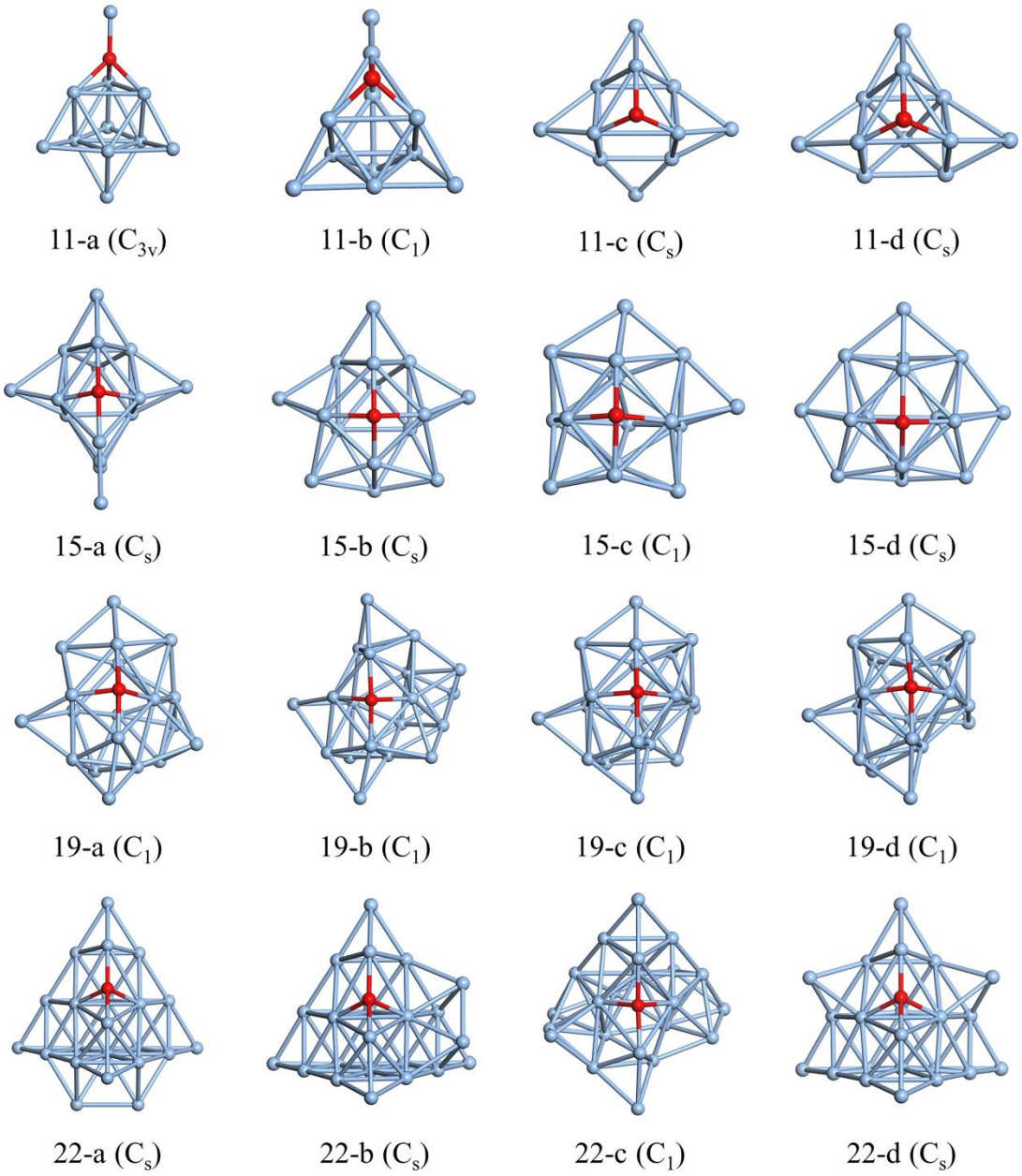

Figure S7. Low-energy structures of $Ag_{11,\ 15,\ 19,\ 22}O^+$ clusters. For each size *n*, the isomers were marked as *n*-b, *n*-c, *n*-d relating to the energy difference with the lowest-energy one (marked as *n*-a). The cluster symmetries are given in brackets. The sliver and oxygen atoms are shown in blue and red, respectively.

Table S4. The geometric and electronic properties of $Ag_{11,\ 15,\ 19,\ 22}O^{+}$ clusters from cam-B3LYP/SDD calculation considering zero point and thermal correction, including energy difference between isomers with G-S at each size *n* (ΔE_{GS}), binding energy per atom (E_b), HOMO-LUMO gap (E_{HL}), average bond length between Ag and O ($R_{Ag\text{-}O}$), average bond length between Ag and Ag ($R_{Ag\text{-}Ag}$), and minimum frequency (υ_{min}).

Cluster	ΔE_{GS} (eV)	E_b (eV)	E_{HL} (eV)	$R_{Ag\text{-}O}$ (Å)	$R_{Ag\text{-}Ag}$ (Å)	υ_{min} (cm^{-1})
11-a	**0.000**	**1.064**	**3.728**	**2.165**	**2.849**	**26.64**
11-b	0.127	1.054	4.544	2.095	2.846	15.84
11-c	0.217	1.046	4.544	2.110	2.844	16.67
11-d	0.246	1.044	4.082	2.106	2.861	16.74
15-a	**0.000**	**1.217**	**3.782**	**2.175**	**2.881**	**14.24**
15-b	0.055	1.214	3.782	2.210	2.896	28.28
15-c	0.140	1.208	3.837	2.222	2.883	20.80
15-d	0.172	1.206	3.837	2.204	2.882	25.53
19-a	**0.000**	**1.308**	**3.755**	**2.181**	**2.855**	**26.31**
19-b	0.044	1.306	3.565	2.185	2.906	24.50
19-c	0.155	1.300	3.565	2.204	2.897	22.96
19-d	0.168	1.299	3.619	2.202	2.918	22.85
22-a	**0.000**	**1.352**	**2.449**	**2.176**	**2.890**	**23.13**
22-b	0.023	1.351	2.476	2.177	2.893	21.03
22-c	0.184	1.344	2.422	2.179	2.906	22.40
22-d	0.195	1.344	2.558	2.179	2.905	26.60

Table S5. The geometric and electronic properties of Ag_nO^+ (n = 7−11, 15, 19, 22) clusters from cam-B3LYP/SDD calculation considering zero point and thermal correction, including average bond length between Ag and O (R_{Ag-O}, in Å), bond length between hanging Ag and O ($R_{Ag(h)-O}$, in Å), average bond length between Ag and Ag (R_{Ag-Ag}, in Å), average Wiberg bond order between the Ag and O except for hanging Ag atom (BO_{Ag-O}), Wiberg bond order between the hanging Ag atom and O ($BO_{Ag(h)-O}$), average Wiberg bond order between Ag and Ag (BO_{Ag-Ag}), *d*-band center (ε_d, in eV), and *s* orbital center (ε_s, in eV).

Cluster	R_{Ag-O}	$R_{Ag(h)-O}$	R_{Ag-Ag}	BO_{Ag-O}	$BO_{Ag(h)-O}$	BO_{Ag-Ag}	ε_d	ε_s
7-a	**2.236**	**2.051**	**2.860**	**0.244**	**0.363**	**0.264**	**−14.23**	**−11.98**
7-b	2.098	2.033	2.842	0.367	0.367	0.288	--	--
8-a	**2.144**	**--**	**2.883**	**0.315**	**--**	**0.222**	**−14.74**	**−12.7**
8-b	2.207	2.056	2.853	0.243	0.329	0.254	**--**	**--**
9-a	**2.120**	**--**	**2.861**	**0.364**	**--**	**0.234**	**−14.57**	**−12.44**
9-b	2.198	2.054	2.836	0.247	0.315	0.287	--	--
10-a	**2.194**	**2.065**	**2.856**	**0.241**	**0.302**	**0.227**	**−13.98**	**−11.54**
10-b	2.148	--	2.879	0.299	--	0.221	--	--
11-a	**2.203**	**2.051**	**2.849**	**0.235**	**0.332**	**0.248**	**−13.76**	**−12.22**
11-b	2.095	--	2.846	0.354	--	0.257	--	--
15-a	**2.175**	**--**	**2.881**	**0.234**	**--**	**0.244**	**−13.77**	**−10.87**
15-b	2.210	--	2.896	0.270	--	0.229	--	--
19-a	**2.181**	**--**	**2.855**	**0.250**	**--**	**0.222**	**−13.62**	**−12.23**
19-b	2.185	--	2.906	0.246	--	0.221	--	--
22-a	**2.176**	**--**	**2.890**	**0.215**	**--**	**0.211**	**−13.51**	**−12.00**
22-b	2.177	--	2.893	0.228	--	0.210	--	--

Table S6. The mixing character of O and silver atoms coordinated with O to the frontier orbitals of Ag_nO^+ (n = 7−11, 15, 19, 22) clusters from cam-B3LYP/SDD calculation considering zero point and thermal correction and analyzed by neutral atomic orbital (NAO) method.

Orbital	HOMO		HOMO−1		HOMO−2		HOMO−3		HOMO−4		HOMO−5		HOMO−6		HOMO-7	
Percent (%)	O	Ag_{Ag-O}	O	Ag_{Ag-O}	O	Ag_{Ag-O}	O	Ag_{Ag-O}	O	Ag_{Ag-O}	O	Ag_{Ag-O}	O	Ag_{Ag-O}	O	Ag_{Ag-O}
7-a	**6.15**	**27.58**	**30.10**	**36.35**	**59.28**	**39.35**	**44.87**	**48.45**	**15.88**	**49.21**	**3.92**	**20.23**	**0.69**	**49.67**	**5.11**	**44.85**
7-b	2.92	22.75	74.57	23.08	42.01	39.03	53.54	44.41	5.76	44.81	0.56	59.09	0.00	82.35	0.00	69.76
8-a	**6.39**	**24.66**	**7.90**	**19.00**	**52.21**	**27.20**	**46.52**	**44.74**	**43.86**	**45.72**	**11.36**	**43.06**	**0.22**	**52.89**	**0.24**	**22.94**
8-b	5.56	41.39	4.04	26.09	31.98	38.55	49.73	45.61	46.46	48.50	10.66	46.85	3.18	32.13	0.63	57.24
8-c	7.22	40.37	1.57	27.47	39.33	37.82	51.23	45.29	46.92	46.35	8.49	46.09	0.34	27.83	1.19	56.42
9-a	**54.47**	**19.65**	**35.41**	**17.06**	**35.39**	**17.07**	**24.07**	**40.60**	**24.05**	**40.62**	**8.90**	**45.58**	**0.00**	**65.45**	**0.56**	**70.42**
9-b	1.56	20.88	6.03	23.32	31.05	36.99	40.48	51.72	50.90	44.96	11.14	43.89	2.27	42.71	1.75	34.75
10-a	**3.48**	**47.46**	**5.15**	**19.07**	**5.16**	**19.09**	**39.49**	**43.33**	**47.56**	**47.38**	**47.47**	**47.43**	**5.50**	**54.13**	**0.00**	**70.81**
10-b	5.70	20.11	8.26	16.29	9.77	14.16	46.19	45.05	44.08	45.63	45.79	33.75	0.53	58.32	4.42	44.91
11-a	**4.47**	**21.66**	**3.15**	**18.53**	**3.17**	**18.52**	**49.14**	**46.17**	**49.08**	**46.23**	**37.43**	**43.89**	**1.84**	**11.89**	**1.84**	**11.87**
11-b	21.92	17.81	44.86	21.69	39.63	33.80	47.52	24.37	9.38	36.35	5.63	27.68	4.11	44.96	5.67	53.62
15-a	**3.46**	**13.26**	**0.20**	**17.86**	**18.75**	**23.92**	**34.38**	**29.14**	**35.29**	**21.23**	**36.30**	**22.17**	**16.00**	**41.30**	**9.27**	**39.03**
15-b	0.61	18.18	3.08	19.76	4.83	19.60	52.21	22.31	41.09	26.42	47.55	25.93	7.67	39.86	6.18	40.46
19-a	**1.46**	**11.12**	**3.88**	**12.90**	**0.74**	**9.85**	**1.02**	**16.76**	**36.65**	**24.98**	**41.04**	**27.48**	**39.77**	**27.96**	**26.17**	**32.12**
19-b	1.84	11.45	4.23	13.04	3.05	15.44	5.89	16.50	46.94	25.52	28.78	27.64	40.65	31.43	23.90	25.89
22-a	**3.05**	**12.81**	**5.89**	**9.05**	**0.36**	**6.09**	**8.69**	**11.99**	**0.35**	**6.88**	**16.30**	**15.90**	**36.13**	**34.26**	**51.63**	**36.80**
22-b	0.77	12.69	6.15	9.19	0.01	14.41	8.71	8.78	0.20	17.73	15.73	21.63	40.79	32.04	41.97	33.58

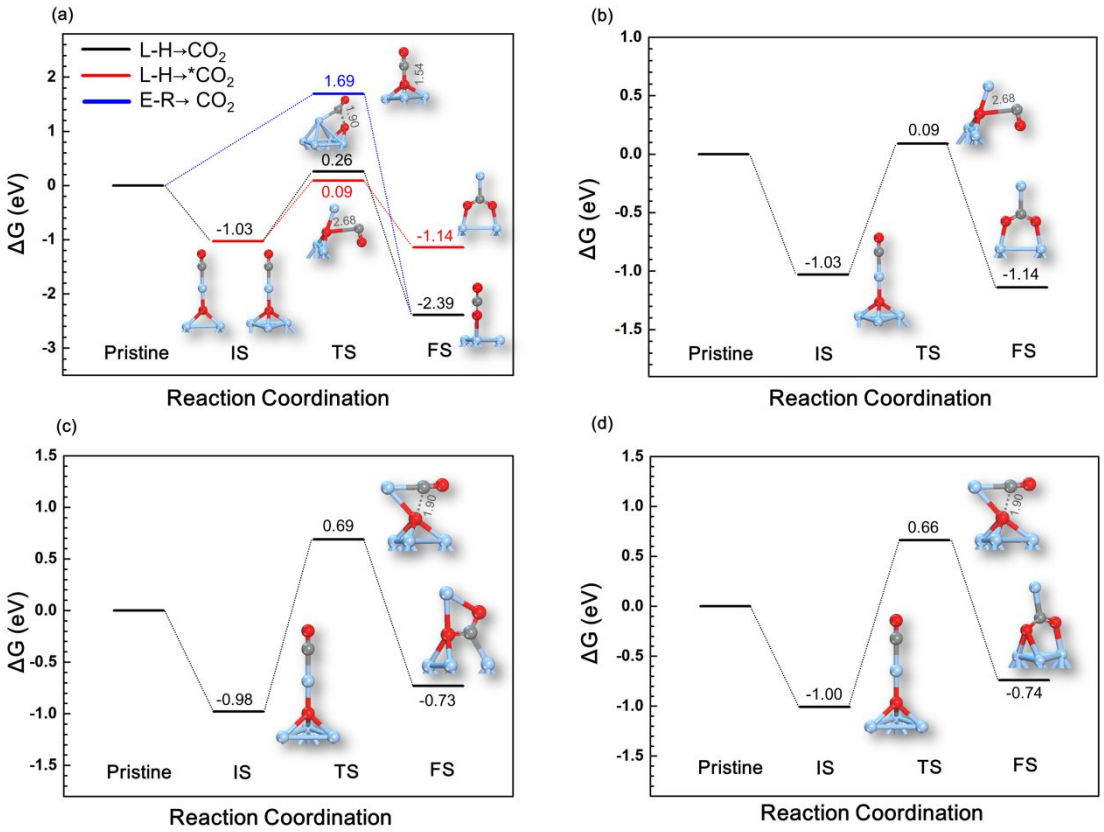

Figure S8. Free energy and corresponding atomic structure of reaction intermediates for the reactions between (a) Ag_8O^+-a; (b) Ag_8O^+-b cluster; (c) $Ag_{10}O^+$-a cluster; (d) $Ag_{11}O^+$-a cluster and CO. Only the Langmuir-Hinshelwood mechanism was considered for Ag-O_{in}-Ag_{n-1}^+ clusters that have inserted O_{in}. Both the Langmuir-Hinshelwood mechanism (pathway 1 in black and pathway 2 in red) and the Eley-Rideal mechanism (in blue) were considered for the clusters having terminal O_{te}.

Table S7. EDA results for Ag_nO^+ (n = 7−11, 15, 19) clusters under the cam-B3LYP/TZP level of theory using ADF 2018.104, taking Ag_n^+ and O as interacting fragments. Energy values are given in eV.

Cluster	ΔE_{pauli}	ΔE_{elstat}	ΔE_{oi}	ΔE_{int}
Ag_7O^+	16.31	−8.52 (31%)	−19.00 (69%)	−11.21
Ag_8O^+-a	12.47	−5.93 (26%)	−17.27 (74%)	−10.72
Ag_8O^+-b	16.57	−8.37 (30%)	−20.00 (70%)	−11.80
Ag_9O^+	13.96	−7.13 (29%)	−17.18 (71%)	−10.35
$Ag_{10}O^+$	17.10	−8.59 (29%)	−20.57 (71%)	−12.07
$Ag_{11}O^+$	17.58	−9.18 (31%)	−20.13 (69%)	−11.73
$Ag_{15}O^+$	16.75	−8.60 (31%)	−19.40 (69%)	−11.26
$Ag_{19}O^+$	16.22	−8.35 (31%)	−18.87 (69%)	−10.99

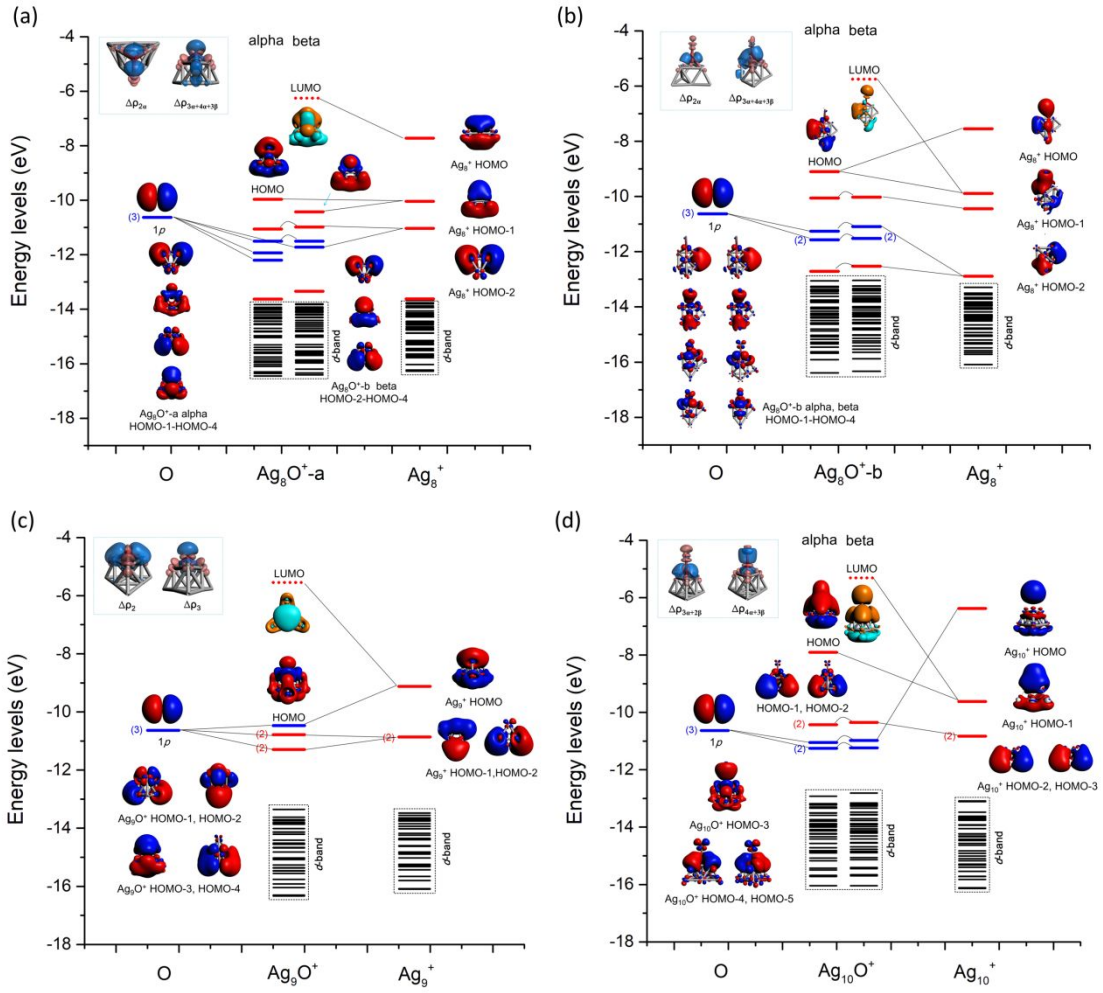

Figure S9. Energy level correlations between $Ag_{8\text{-}10}O^+$ clusters, O atom, and $Ag_{8\text{-}10}^+$ fragments, and electron cloud distributions of frontier orbitals of these clusters. Blue and red colors denote positive and negative phases of the wave function, respectively. Top left insets display the electron deformation density plots (Δρ) of NOCV pairwise orbital interactions between $Ag_{8\text{-}10}^+$ and O fragments calculated at the cam-B3LYP/TZP level of theory using ADF 2018.104. The electrons transfer from light blue to light red. The isosurface values for electron cloud distribution and deformation electron density are ± 0.014 a.u. and ± 0.0015 a.u., respectively.

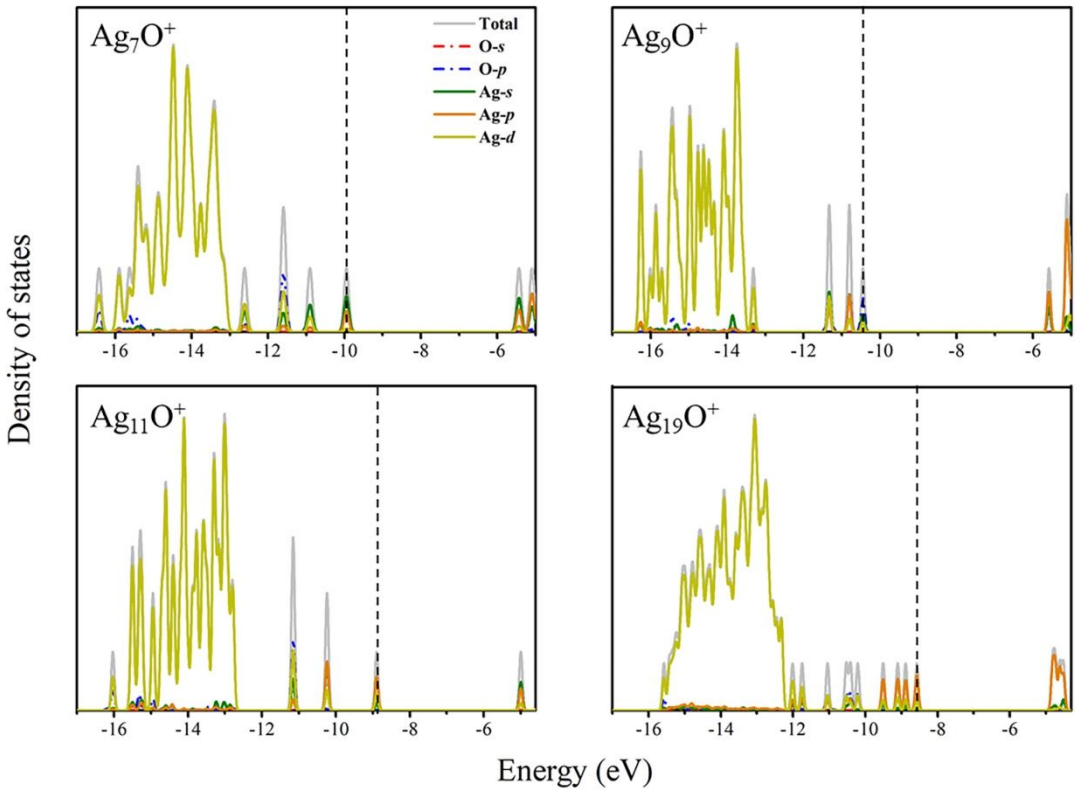

Figure S10. Total (solid light grey) and partial densities of states (PDOS) (*s, p* of O are in dash red, blue, respectively; *s, p, d* of Ag are in solid green, orange, yellow, respectively.) of the $Ag_{7,\ 9,\ 11,\ 19}O^{+}$-a clusters. Orbital energies are calculated at the cam-B3LYP/SDD level of theory considering zero point and thermal correction. The black dotted line marks the HOMO level of each cluster.

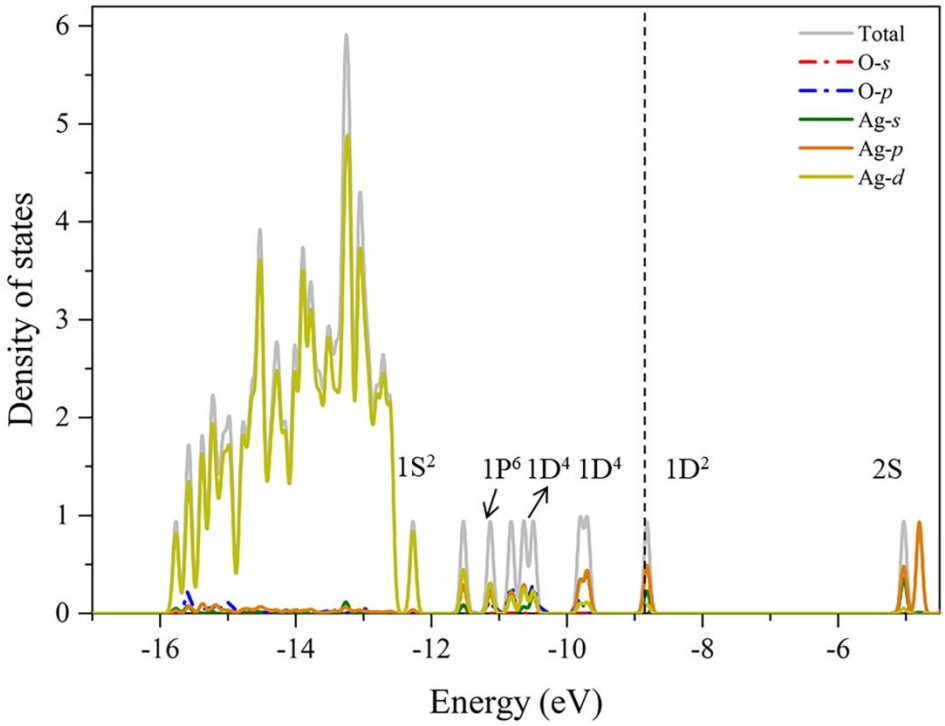

Figure S11. Total (solid light grey) and PDOSs (*s, p* of O are in dash red, blue, respectively; *s, p, d* of Ag are in solid green, orange, yellow, respectively.) of the $Ag_{15}O^{+}$-a cluster. Orbital energies are calculated at the cam-B3LYP/SDD level of theory considering zero point and thermal correction. Molecular orbitals are shown and assigned based on comparison with phenomenological shell model orbitals. The black dotted line marks the HOMO level.

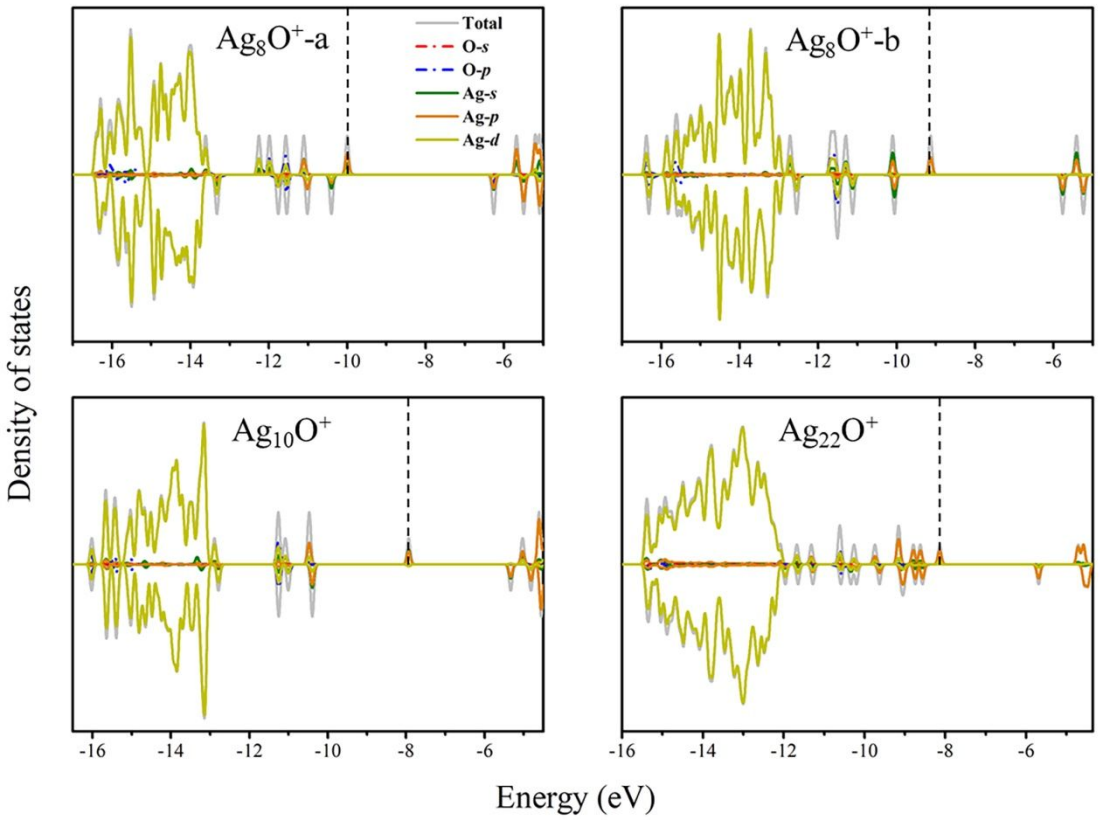

Figure S12. Total (solid light grey) and PDOSs (*s, p* of O are in dash red, blue, respectively; *s, p, d* of Ag are in solid green, orange, yellow, respectively.) of the Ag_8O^+-a, Ag_8O^+-b, $Ag_{10,\ 22}{}^+$-a clusters. Orbital energies are calculated at the cam-B3LYP/SDD level of theory considering zero point and thermal correction. The black dotted line marks the HOMO level of each cluster.

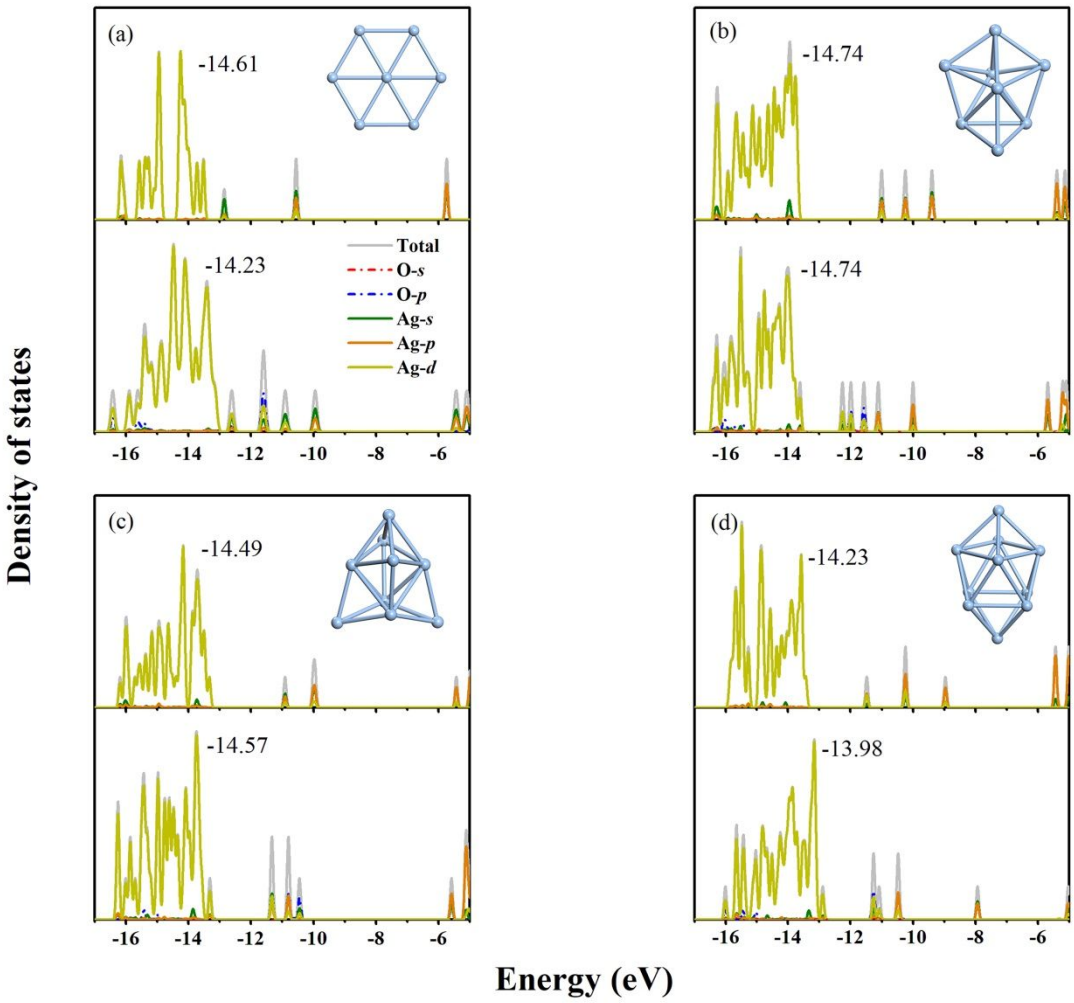

Figure S13. The compared PDOSs between (a) pure Ag_7^+ with Ag_7O^+ cluster; (b) pure Ag_8^+ with Ag_8O^+ cluster; (c) pure Ag_9^+ with Ag_9O^+ cluster; (d) pure Ag_{10}^+ with $Ag_{10}O^+$ cluster. The insets in PDOS are the corresponding structure of each pure $Ag_{7\text{-}10}^+$ clusters. The values are *d*-band center energies for each cluster.

Table S8. EDA-NOCV results for Ag_nOCO^+ (n = 7−11, 15) complexes under the cam-B3LYP+D3/TZP level of theory using ADF 2018.104, taking Ag_nO^+ cluster and CO molecular as interacting fragments. Energy values are given in eV.

	Ag_7O^+	Ag_8O^+-a	Ag_8O^+-b	Ag_9O^+	$Ag_{10}O^+$	$Ag_{11}O^+$	$Ag_{15}O^+$
ΔE_{int}	−1.24	−2.08	−2.11	−1.17	−1.85	−1.18	−0.36
ΔE_{pauli}	4.28	4.45	4.41	4.56	4.82	4.94	3.35
ΔE_{elstat}	−3.74	−3.88	−3.77	−3.90	−3.91	−4.16	−2.55
ΔE_{dist}	0.40	−0.36	−0.46	0.42	−0.33	0.41	0.30
ΔE_{oi}	−2.17	−2.30	−2.29	−2.26	−2.43	−2.38	−1.46
$\Delta E_{oi(\sigma\text{-donation})}$	−1.14	−0.35	−0.48	−1.14	−0.47	−1.20	−0.63
$\Delta E_{oi(\pi\text{-back donation})}$	−1.02	−1.83	−1.68	−1.10	−1.81	−1.16	−0.20
$\Delta E_{oi(rest)}$	−0.02	−0.11	−0.13	−0.02	−0.15	−0.01	−0.64

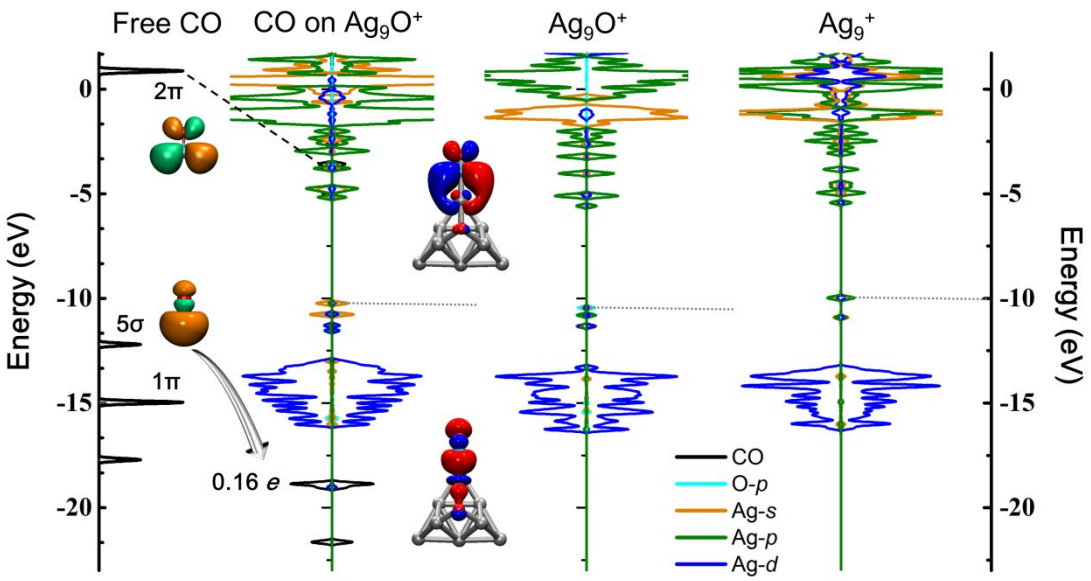

Figure S14. From left to right: DOS (or PDOS) of free CO molecule, CO chemisorbed on the Ag_9O^+ cluster, the pristine Ag_9O^+ and the Ag_9^+ cluster, respectively. The insets display the electron cloud distributions of CO and Ag_9O^+ orbitals. The isosurface value is ± 0.04 a.u. The light grey dash line marked the HOMOs of Ag_9OCO^+ complex, Ag_9O^+, and Ag_9^+ cluster, respectively.

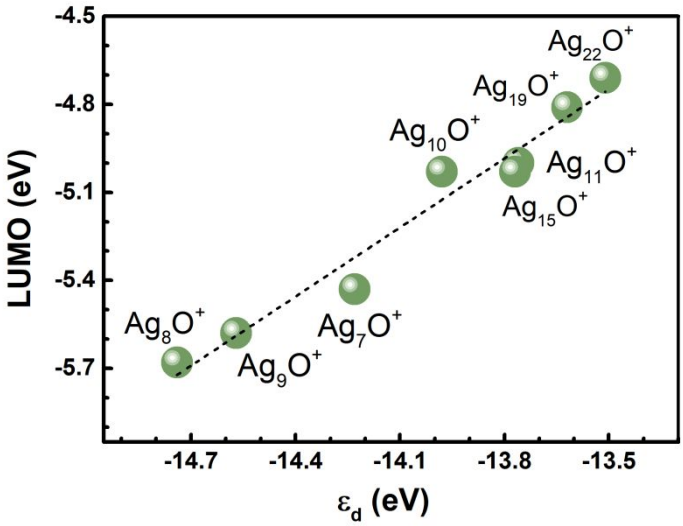

Figure S15. LUMO as a function of ε_d *d*-band center of Ag_nO^+ clusters.

Table S9. The geometric and electronic properties of $Ag_{7\text{-}11,\ 15}O^+$ clusters from cam-B3LYP/aug-cc-pVDZ-pp/Ag/6-311G(d)/C/O calculation considering D3 correction, including the NPA charge of O atom of cluster (Q_O, in e), active Ag site of cluster (Q_{Ag*}, in e), C atom of CO ($Q_{CO\text{-}C}$, in e), O atom of CO ($Q_{CO\text{-}O}$, in e); average bond length between Ag and O ($R_{Ag\text{-}O}$, in Å), bond length between active Ag site and C ($R_{Ag*\text{-}C}$, in Å), and bond length between C and O of CO ($R_{C\text{-}O(CO)}$, in Å).

Reaction	Q_O	Q_{Ag*}	$Q_{CO\text{-}C}$	$Q_{CO\text{-}O}$	$R_{Ag\text{-}O}$	$R_{Ag*\text{-}C}$	$R_{C\text{-}O(CO)}$
gas CO	--	--	0.469	−0.469	--	--	1.122
7-a	−1.348	0.814	--	--	2.182	--	--
*CO	−1.308	0.599	0.503	−0.344	2.174	1.988	1.118
TS	−1.307	0.794	0.587	−0.552	2.219	2.789	1.170
$*CO_2$	−0.730	0.578	0.508	−0.848	2.260	2.105	1.292
8-a	−1.066	0.580	--	--	2.120	--	--
	−1.252	0.599	0.499	−0.354	2.047	1.977	1.119
*CO	−1.296	0.619	0.502	−0.343	2.153	1.990	1.118
$TS_{L-H\rightarrow co_2}$	−0.667	0.241	0.515	−0.402	2.262	2.262	1.162
$TS_{L-H\rightarrow *co_2}$	−1.309	0.795	0.533	−0.483	2.105	2.617	1.161
$TS_{E-R\rightarrow co_2}$	−0.971	0.400	0.970	−0.344	2.123	3.115	1.122
$*CO_2$	−0.755	0.552	0.537	−0.755	2.118	2.111	1.257
CO_2	−0.555	0.243	1.057	−0.442	*2.520*	5.428	1.146
8-b	−1.335	0.834	--	--	2.161	--	--
*CO	−1.296	0.619	0.502	−0.343	2.153	1.990	1.118
TS	−1.309	0.795	0.533	−0.483	2.079	2.615	1.161
$*CO_2$	−0.755	0.552	0.537	−0.755	2.118	2.111	1.257
9-a	−1.164	0.446	--	--	2.103	--	--
*CO	−1.198	0.594	0.514	−0.355	2.068	1.982	1.120
TS_{L-H}	−1.176	0.243	0.523	−0.429	2.195	2.251	1.164
TS_{E-R}	−1.014	0.246	0.983	−0.358	2.105	3.225	1.122
CO_2	−0.488	0.084	1.042	−0.488	--	3.400	1.156
10-a	−1.325	0.323	--	--	2.153	--	--
*CO	−1.290	0.627	0.503	−0.347	2.144	1.990	1.118
TS	−1.228	0.822	0.456	−0.474	2.264	2.225	1.178
$*CO_2$	−0.716	0.564	0.538	−0.833	2.261	2.108	1.287
11-a	−1.330	0.822	--	--	2.153	--	--
*CO	−1.296	0.625	0.504	−0.348	2.148	1.988	1.119

TS	−1.226	0.815	0.442	−0.450	2.250	2.148	1.141
*CO_2	−0.845	0.551	0.535	−0.725	2.223	2.104	1.242
15-a	−1.252	0.326	--	--	2.164	--	--
*CO	−1.235	0.152	0.551	−0.383	2.168	2.161	1.120

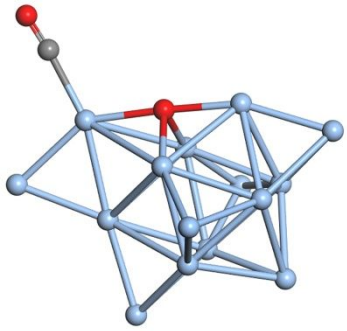

$\Delta G = -0.09$ eV

Figure S16. Free energy and corresponding atomic structure for CO adsorbed on $Ag_{15}O^{+}$-a cluster.

Reference:

(1) Frisch, M.; Trucks, G.; Schlegel, H.; Scuseria, G.; Robb, M.; Cheeseman, J.; Scalmani, G.; Barone, V.; Petersson, G.; Nakatsuji, H., Gaussian 16, Revision A. 03, Gaussian. *Inc., Wallingford CT* **2016**.

(2) Zhao, J. J.; Shi, R. L.; Sai, L. W.; Huang, X. M.; Su, Y., Comprehensive Genetic Algorithm for Ab Initio Global Optimisation of Clusters. *Mol. Simul.* **2016**, *42*, 809-819.

(3) Fonseca Guerra, C.; Snijders, J. G.; te Velde, G.; Baerends, E. J., Towards an Order-N Dft Method. *Theor. Chem. Acc.* **1998**, *99*, 391-403.

(4) te Velde, G.; Bickelhaupt, F. M.; Baerends, E. J.; Fonseca Guerra, C.; van Gisbergen, S. J. A.; Snijders, J. G.; Ziegler, T., Chemistry with Adf. *J. Comput. Chem.* **2001**, *22*, 931-967.

(5) Baerends, E. J. Z., T.; Autschbach, J.; Bashford, D.; Bérces, A.; Bickelhaupt, F.; Bo, C.; Boerrigter, P.; Cavallo, L.; Chong, D., Adf2018, Scm, Theoretical Chemistry, Vrije Universiteit, Amsterdam, the Netherlands. http://www.scm.com. (accessed Oct 24, 2018).

(6) Zhao, L. L.; von Hopffgarten, M.; Andrada, D. M.; Frenking, G., Energy Decomposition Analysis. *WIRES Comput. Mol. Sci.* **2018**, *8*, 37.

(7) Zhao, L. L.; Hermann, M.; Schwarz, W. H. E.; Frenking, G., The Lewis Electron-Pair Bonding Model: Modern Energy Decomposition Analysis. *Nat. Rev. Chem.* **2019**, *3*, 48-63.

(8) Mitoraj, M. P.; Michalak, A.; Ziegler, T., A Combined Charge and Energy Decomposition Scheme for Bond Analysis. *J. Chem. Theory Comput.* **2009**, *5*, 962-975.

(9) Ghosh, A.; Chaudhuri, R. K.; Chattopadhyay, S., Relativistic State-Specific Multireference Coupled Cluster Theory Description for Bond-Breaking Energy Surfaces. *J. Chem. Phys.* **2016**, *145*, 124303.

(10) Meunier, A.; Lévy, B.; Berthier, G., Corrélation lectronique Et Effets De Base Dans L'étude De La Liaison Hydrogène: Le Dimère Mixte Ammoniac-Eau. *Theor. Chim. Acta* **1973**, *29*, 49-55.